Hindawi
Journal of Nanomaterials
Volume 2019, Article ID 7921273, 15 pages
https://doi.org/10.1155/2019/7921273

Research Article

Shape Tuning of Magnetite Nanoparticles Obtained by Hydrothermal Synthesis: Effect of Temperature

Nayely Torres-Gómez,[1] Osvaldo Nava,[2] Liliana Argueta-Figueroa,[3] René García-Contreras,[4] Armando Baeza-Barrera,[5] and Alfredo R. Vilchis-Nestor[1]

[1]*Centro Conjunto de Investigación en Química Sustentable, UAEM-UNAM, Facultad de Química, UAEM, Toluca 50120, Mexico*
[2]*Facultad de Ingeniería, Arquitectura y Diseño-Universidad Autónoma de Baja California, 22860 Ensenada, B.C., Mexico*
[3]*Cátedras CONACYT, Facultad de Odontología, Universidad Autónoma Benito Juárez de Oaxaca, Oaxaca 68120, Mexico*
[4]*Laboratorio de Investigación Interdisciplinaria, Área de Nanoestructuras y Biomateriales, Escuela Nacional de Estudios Superiores Unidad León, Universidad Nacional Autónoma de México; León, Guanajuato 37684, Mexico*
[5]*Tecnológico Nacional de México, Instituto Tecnológico de Toluca, Av. Tecnológico s/n. Fraccionamiento La Virgen, Metepec, Mexico*

Correspondence should be addressed to Alfredo R. Vilchis-Nestor; arvilchisn@uaemex.mx

Received 1 June 2018; Accepted 28 October 2018; Published 7 February 2019

Academic Editor: Paulo Cesar Morais

In this work, we present a simple and efficient method for pure phase magnetite (Fe_3O_4) nanoparticle synthesis. The phase structure, particle shape, and size of the samples were characterized by Raman spectroscopy (Rm), X-ray diffraction (XRD), scanning electron microscopy (SEM), energy-dispersive X-ray (EDS), and transmission electron microscopy (TEM). The morphology tuning was controlled by the temperature of the reaction; the nanoparticles were synthesized via the hydrothermal method at 120°C, 140°C, and 160°C, respectively. The Rm and XRD spectra showed that all the nanoparticles were Fe_3O_4 in a pure magnetite phase. The obtained nanoparticles exhibited a high level of crystallinity with uniform morphology at each temperature, as can be observed through TEM and SEM. These magnetic nanoparticles exhibited good saturation magnetization and the resulting shapes were quasi-spheres, octahedrons, and cubes. The samples showed striking magnetic properties, which were examined by a vibrating sample magnetometer (VSM). It has been possible to obtain a good morphological control of nanostructured magnetite in a simple, economical, and scalable method by adjusting the temperature, without the modification of any other synthesis parameter.

1. Introduction

Finding a novel and simple approach in order to obtain architecturally controlled magnetic nanocrystals is a significant challenge toward the production of future nanodevices. Different iron oxides have been applied in many fields, but one that draws much attention for its magnetic properties is magnetite, mainly due to the presence of cations in two different states of oxidation within the same crystal lattice [1–6], also due to it having different characteristics at a nanostructural level, depending on the morphology and size of the particles, which can be exploited in both medicine and biotechnology [7–10].

There are several synthesis methods used to produce magnetite nanoparticles. The most used method to obtain magnetite nanoparticles is coprecipitation which usually employs Fe^{2+} and Fe^{3+} chlorides, as precursor salts, with an ammonium hydroxide solution. This process is simple and fast; nevertheless, the presence of more than one iron oxide phase is a common problem; size control is difficult to achieve, and furthermore, shape tuning is a huge challenge [11–13]. Despite this, some variations have been proposed to improve the viability of the coprecipitation method; it has only been possible to obtain nanoparticles with an acceptable size distribution and phase control using other precursor salts or oxidizing agents, but morphological

control remains difficult. Other approaches are thermal decomposition [14–16] and the reduction of α-Fe_2O_3 dispersed in a hydrogen stream at elevated temperatures [17, 18], with which nanoparticles of approximately 10 and 50 nm, respectively, can be produced. The solvothermal methods deserve a special mention because of the uniform size of the nanoparticles that can be obtained; this method typically employs a mixture of $FeCl_3$, ethylene glycol, and sodium acetate, which are allowed to react in an autoclave [19, 20].

The hydrothermal/solvothermal methods have been reported to present a better morphological control [21, 22]. With the hydrothermal synthesis, the following products can be obtained: (a) synthesis of new phases or stabilization of new complexes; (b) crystalline growth of several inorganic compounds; and (c) preparation of nanostructured and single-crystal materials with well-defined size and morphology, for their use in specific applications. This method is the most efficient to synthesize nanocrystals because it exploits the solubility of some inorganic substances at certain temperatures and high pressures. This later favors the crystallization of the dissolved materials within the fluid since temperature, pressure, and reaction time are the three main physical parameters that need to be controlled or manipulated in order to maintain good nucleation and particle distribution [23].

As stated, several variables must be controlled during Fe_3O_4 synthesis. However, the most important one to avoid would be the material rusting and changing its phase to one of the most stable oxides in an oxidizing environment, hematite. To achieve this, you can work in an inert atmosphere and/or use a variety of surfactants in order to protect the surface from oxidation [24–26]. Of these surfactants, polyethylene glycol (PEG) stands as the most used when the desired material must be applied in the field of medicine due to it is biocompatibility and low cost [27–29].

To date, Fe_3O_4 nanoparticles have been synthesized with various morphologies such as sphere, cube, and wire, among others. We focused our study of existing literature on the control of the morphology by changing two or three variables (temperature, solvent, precursor salt, reducing agent, etc.) simultaneously within a hydrothermal or solvothermal reaction and through the use of surfactants [30–37].

There are interesting biological applications for iron oxides, taking advantage of their inherent magnetic properties. Since magnetic iron oxide nanoparticles coated with PEG usually exhibit good biocompatibility, they can be used for biological applications and are widely applied in drug delivery carriers [38], magnetic resonance imaging contrast agents [39], and hyperthermia for cancer cells [40], although it is still imperative to test the biological effect of these magnetic nanostructures on microorganisms and human cell lines *in vitro*.

In this work, a simple and easy to reproduce method was developed to synthesize nanostructured magnetite by means of hydrothermal synthesis. The different resulting morphologies were obtained by changing the reaction temperature (120, 140, and 160°C), without changing any other parameter in the synthesis, taking advantage of the relationship between temperature, reaction kinetics, and nucleation rates. In addition, the antibacterial and cytotoxic activities of the different resulting morphologies of magnetite nanoparticles were determined.

2. Experimental Section

2.1. Materials. Iron (III) chloride hexahydrate ($FeCl_3{\cdot}6H_20$), polyethylene glycol (PEG 8000), and hydrazine 64% (N_2H_4) were purchased from Sigma-Aldrich, while ethanol (EtOH) was purchased from Fermont. All the chemical reagents used in this synthesis were of reactive grade without further purification. Deionized water was employed throughout all of the syntheses.

2.2. Methodology. The Fe_3O_4 nanostructures were synthesized based on previous studies [41] with the following modifications.

A solution of 30 mL water containing $FeCl_3{\cdot}6H_20$ (28 mM) and PEG (0.3 mM) was prepared under magnetic stirring. Subsequently, 3 mL of N_2H_4 was added dropwise, while the solution was stirred vigorously with a magnetic stirrer. At the end of the hydrazine addition, a reddish solution was obtained, which was then transferred immediately to different Teflon autoclaves and heated at different temperatures (120°C, 140°C, and 160°C) in a muffle furnace for 4 hours. Finally, the nanostructures were collected with a magnet and washed three times with deionized water and ethanol, then dried at 70°C for 24 hours before further characterization and use.

2.3. Characterization

2.3.1. Raman Spectroscopy. For Rm characterization, a drop of the sample of magnetite nanoparticles dispersed in water was placed on a glass slide and dried at 40°C for one hour. The Rm spectra were obtained using Micro-Raman LabRaman model HR-800 Jobin-Yvon Horiba with a spectral resolution of 2 cm^{-1} on a He-Ne laser (632.8 nm); the power of the laser was 25 μW.

2.3.2. X-Ray Diffraction. The X-ray diffraction patterns (XRD) were collected on a PANalytical X'Pert Pro Diffractometer MPD with a Cu-Kα source and a 2θ ranging from 25° to 70°.

2.3.3. Scanning Electron Microscopy and Energy-Dispersive X-Ray. For the scanning electron microscopy (SEM) analysis, Fe_3O_4 NPs were dispersed in isopropyl alcohol from which a drop was taken and placed on a silicon wafer, to be observed in a FEG Hitachi S-5500 ultra-high-resolution electron microscope (0.4 nm at 15 kV) with a BF/DF Duo STEM detector. A JEOL JSM-6510LV, operated at an acceleration voltage of 20 kV, with a tungsten filament, is attached to an oxford energy scattering probe with a resolution of 137 eV, where the energy-dispersive X-ray (EDS) studies were carried out.

2.3.4. Transmission Electron Microscopy, High-Resolution Transmission Electron Microscopy, and Selected Area Electron Diffraction. One drop of each sample, dispersed in

isopropyl alcohol, was placed in a copper grid coated with carbon, then let to air dry in order to be analyzed in the TEM microscope, a JEOL JEM-2010F equipped with a field emission gun and operated at 200 kV with 0.1 nm lattice resolution, which carried out the TEM and HRTEM studies. A JEOL-2100 with a LaB_6 filament was used to perform the SAED studies.

2.3.5. Magnetic Measurements. Magnetic measurements were run at room temperature using a magnetometer (Versalab Crio Free VSM, Quantum Design) with a maximum applied field of $H_{max} = 20$ kOe.

2.3.6. Antibacterial Activity. For the antibacterial activity, we followed the methods of Argueta-Figueroa et al. [42]. The bacterial strains used in this study were provided by Facultad de Medicina, Universidad Nacional Autónoma de México (UNAM). The strains used are endemic to the region of central Mexico and each one was characterized by a battery of cultural and biochemical tests. The experiments on the antimicrobial activity were carried out as described by the Clinical and Laboratory Standards Institute [43]. Antimicrobial activity of the Fe_3O_4 nanoparticles was tested against the human pathogenic bacteria *Staphylococcus aureus* (*S. aureus*), *Escherichia coli* (*E. coli*), and *Enterococcus faecalis* (*E. faecalis*) by determining the minimal inhibitory concentration (MIC) and the minimal bactericidal concentration (MBC), following the broth dilution method. Selective media were used to culture each strain and were afterwards cultivated in nonselective medium. Each strain was incubated at 37°C for 24 h for the fresh bacterial cultures, which were used to prepare McFarland standards. McFarland standards were diluted in a 1 : 20 relation using saline solution. In 96-well microplates, 100 μL of Mueller-Hinton broth medium (Sigma-Aldrich, St. Louis, MO, USA) was placed in each well, and then 100 μL of the synthesized Fe_3O_4 nanoparticles (quasi-spheres, octahedrons, or cubes, respectively) at a concentration of 5 mg/mL, (previously dissolved in Mueller-Hinton broth and sonicated for 30 min) was stirred in. At this point in time, serial dilutions were performed. We used a positive growth control for the bacteria and a negative growth control for the sterile broth and the nanoparticles. Each well was inoculated aseptically with 5 μL of the respective bacterial suspension (the final concentration was approximately 5×10^5 CFU/mL). Tests were performed in four wells for each concentration and strain. The inoculated microplates were incubated at 37°C for 24 h and stirred at 200 rpm in an incubator. The supernatant was transferred to new 96-well microplates to avoid interference with the reading due to the precipitated nanoparticles. Optical density was read on a microplate reader (Thermo Scientific, St. Louis, MO, USA) at 595 nm. The results were expressed as a percentage of the viable bacteria compared with the untreated controls. A minimal concentration, that showed no turbidity (absence of turbidity at naked eye), was recorded as the MIC of the Fe_3O_4 nanoparticles. 5 μL of dilution from the wells was subcultured on Mueller-Hinton agar plates to corroborate the data obtained from the aforementioned optical density reading.

2.3.7. Cytotoxicity Evaluation

(1) Cell Culture. In order to evaluate the cytotoxicity, we followed the methods reported by Argueta-Figueroa et al. [42], as follows: human gingival fibroblast (HGF), human pulp cells (HPC), and human bone cells (HBC) were prepared from gingival, pulp, and bone tissues obtained from a 25-year-old patient based on prior written informed consent and approval from the bioethics committee of the Escuela Nacional de Estudios Superiores (ENES) Unidad León, UNAM. Tissues were cut into small fragments using a surgical blade and fragments were seeded onto 10 cm culture dishes and cultured in an Alpha Modification of Eagle's Medium (α-MEM, Life Technologies Gibco, Carlsbad, CA, USA) supplemented with 20% fetal bovine serum (FBS, Life Technologies Gibco), 100 UI/mL penicillin, 100 mg/mL streptomycin (FBS, Life Technologies Gibco), and 1% of Glutamax (Life Technologies Gibco). The primary cultures were incubated at 37°C in a humidified atmosphere of 5% CO_2 until the cell population covered 80% of the plate, approximately at 21 days of cultivation. Cells were then harvested by treatment with 0.25% trypsin-0.025% EDTA-2Na in PBS and either subcultured or used for experiments. Cells were subcultured in Dulbecco's Modified Eagle Medium (DMEM, Life Technologies Gibco) supplemented with 10% FBS and antibiotics under 95% of humidified atmosphere with 5% CO_2.

(2) Assay for Cytotoxic Activity. HGF, HPC, and HBC (1×10^5 cells/mL) were inoculated into each well of 96-microwell plates and incubated for 48 h to achieve complete cell adherence and proliferation. The different Fe_3O_4 nanoparticles (quasi-spheres, octahedrons, or cubes) were inoculated at different concentrations at 5, 2.5, 1.25, 0.625, 0.3125, 0.15625, and 0.078125 mg/mL and incubated for a further 24 h. The relative viable cell count was determined by the MTT assay (Sigma-Aldrich, St. Louis, MO, USA). Afterwards, the culture medium was replaced with 3-(4,5-dimethylthiazol-2-yl)-2,5-diphenyltetrazolium bromide (MTT) (0.2 mg/mL) dissolved in DMEM, and cells were incubated for 4 h at 37°C. After replacing the medium, the formazan product was dissolved in dimethyl sulfoxide (DMSO, Sigma-Aldrich, St. Louis, MO, USA). As viable cells remain in the bottom of the wells, the supernatant was therefore removed and the cells washed three times before the well readings were carried out. The optical absorbance at 570 nm of the lysate was determined by using a microplate reader (Thermo Scientific, St. Louis, MO, USA). The cytotoxicity test was performed for each nanoparticle sample in triplicate independent experiments according to ISO 10990-5 Biological evaluation of medical devices—Part 5: Tests for in vitro cytotoxicity.

3. Results and Discussion

Figure 1 shows a photograph of the particles dispersed in water; here the characteristic dark color of the magnetite and the appropriate response to contact with a magnet are observed. In Figure 1(b), it can be seen that the particles are

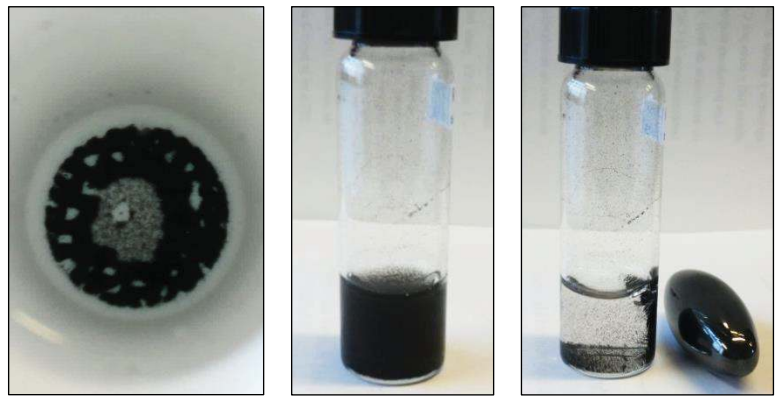

(a) (b) (c)

Figure 1: Photograph of nanoparticles obtained at synthesis hydrothermal at 140°C.

stable in colloidal solution. This behavior is the same for all samples.

3.1. Raman Spectroscopy. Rm spectroscopy is a characterization technique used to accurately identify different iron oxide phases within the samples. Magnetite has an inverse spinel structus above 119°K, resulting in five Raman bands: three T_{2G}, one A_{1g}, and one E_g, respectively [44]. While in ambient conditions, the nonpolarized spectra of magnetite show four of the five bands at 668, 538, 306, and 193 cm^{-1}, the last one appears very weakly and has only been reported a few times [45]. A summary of the Raman shift associated with magnetite is shown in Table 1.

After the nanoparticle suspensions were dripped on glass slides, Rm spectra of three samples were collected (as shown in Figure 2) using a low laser intensity (25 μW) in order to prevent oxidation of the samples caused by overheating. Although laser intensity is required to improve the high quality of the Rm spectra, the use of a considerably larger intensity has been found to oxidize the samples of magnetite, even when the nanoparticles are coated. This can affect the crystalline structure, and the Raman bands associated with hematite could appear at 226, 245, 292, 411, 497, and 612 cm^{-1} [52].

Figure 2 shows the Rm spectra of the magnetite nanoparticles synthesized of three different temperatures. The vibrational spectra analysis can be described based on the structure of the spinel magnetite. In Figure 2, the most intense band observed in all three samples is centered at 667 cm^{-1}, and it corresponds to the symmetrical stretching of the oxygen atoms along the Fe-O bonds in the tetrahedral sites of the molecule (A_{1g}). The difference in intensity may be associated with particle morphology as the band at around 540 cm^{-1} can be associated to the asymmetrical stretching of the Fe-O bond (T_{2G}). However, the intensity is too low which suggests that some PEG remains on the surface of the nanoparticle.

3.2. X-Ray Diffraction. The presence of other iron oxide phases, like maghemite, remains a challenge for many synthetic methods. Furthermore, the structural characterization of these materials with nanometric regime must be supported by several techniques in order to identify the present phases, in addition to the size and morphology of the nanoparticles. For this reason, in order to support the Raman studies, the

Table 1: Raman mode frequencies reported in literature for magnetite.

Reference	Raman shift (cm^{-1})	
	Fe-O symmetrical stretching	Fe-O asymmetrical stretching
Boucherit et al. [46]	670	550
Ohtsuka et al. [47]	665	540
Thierry et al. [48]	670	550
De Faria et al. [49]	662.7	533.6
Li et al. [50]	665	540
Bersani et al. [51]	666	541
Present study	**667**	**540**

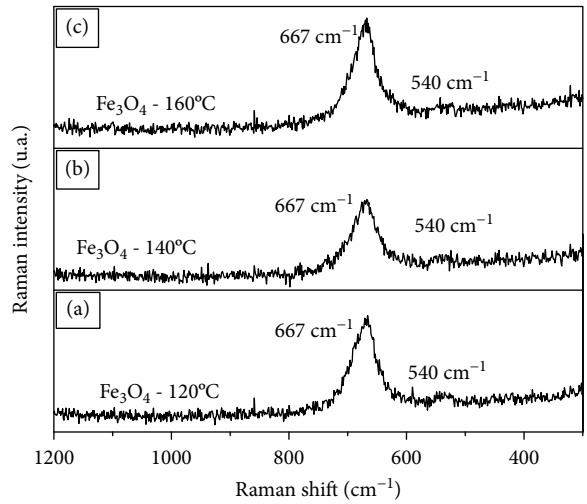

Figure 2: Rm spectra of magnetite nanoparticles synthesized at different temperatures. (a) 120°C. (b) 140°C. (c) 160°C.

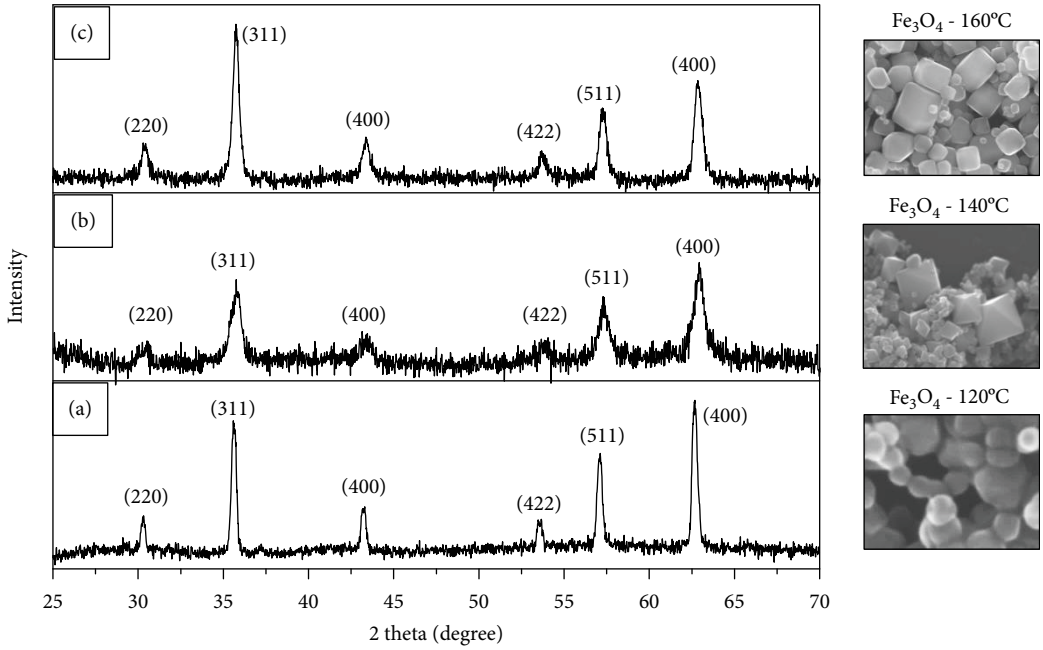

Figure 3: XRD patterns of Fe_3O_4 nanoparticles at different temperatures. (a) 120°C. (b) 140°C. (c) 160°C.

samples were also analyzed by XRD to complement phase identification of the iron oxide in all three samples.

The XRD patterns of the magnetite nanoparticles synthetized at different temperatures, which are shown in Figure 3, reveal that the 2θ diffraction peaks at 30.38°, 35.72°, 43.40°, 53.70°, 57.28°, and 62.79° can be indexed as the (220), (311), (400), (422), (511), and (440) reflections, respectively, corresponding to the cubic spinel structure of magnetite (Fe_3O_4). These characteristic peaks were a perfect match with the standard JCPDS card no. 19-0629, associated with a face center cubic (FCC) cell structure with a lattice constant of $a = 8.393$ Å and a Fd3m space group. Here, half of the trivalent ions (Fe^{3+}) are in the tetrahedral (A) sites, and the other half of the trivalent and all the divalent ions (Fe^{2+}) are randomly distributed in the octahedral (B) interstices. The parallel alignment of Fe^{2+} and Fe^{3+} ions spins in adjacent octahedral sites which leads to a net magnetization and a ferrimagnetic behavior.

In the XRD pattern in Figure 3(b), which corresponds to the magnetite synthesized at 140°C, it can be seen that the diffraction peaks are wider than those of the other two samples. This profile can be explained by considering a large crystallite size range, the presence of lattice strain, a crystallite imperfection (micro strains, d-spacing fluctuations, stacking faults), and/or instrumental defects [53]. Furthermore, geometrical properties and size polydispersity of this sample can add variables that also cause a broadening of the Bragg reflection.

3.3. Scanning Electron Microscopy and Energy-Dispersive X-Ray. Table 2 shows the elemental analysis obtained via EDS studies of the magnetite nanoparticles synthesized at different temperatures, with which we can confirm the presence of each of the elements that make up the material.

Table 2: EDS analysis data of the Fe_3O_4 nanoparticles.

Element	120°C %w	140°C %w	160°C %w
C	15.11	14.16	14.38
O	43.37	44.18	44.37
Fe	**41.52**	**41.66**	**41.25**
Total	100.00	100.00	100.00

The following results were obtained by weight percent (%w): Fe %w was associated with iron oxide, C %w to the surfactant, and O %w was associated in part to the oxide and another part to the surfactant.

The morphology of the nanoparticles obtained in synthesis at the different temperatures was observed by SEM, as seen in Figure 4. The sample synthesized at 120°C presents a nonuniform morphology where the majority of the observable shapes are polyhedral or quasi-spherical (Figures 4(a) and 4(d)). Well-defined octahedral particles are shown in the micrographs of the particles synthesized at 140°C (Figures 4(b) and 4(e)). When synthesis occurs at 160°C, a contrasting morphology of predominantly truncated cubes can be seen (Figures 4(c) and 4(f)).

Although the three syntheses were performed under the same conditions, only varying the reaction temperature, the change in morphology is notorious. This can be explained by the nucleation rate of chemical species due to higher temperatures promoting more collisions between particles, leading into larger and more homogeneously shaped particles.

3.4. Transmission Electron Microscopy, High-Resolution Transmission Electron Microscopy, and Selected Area Electron Diffraction. The results obtained through both

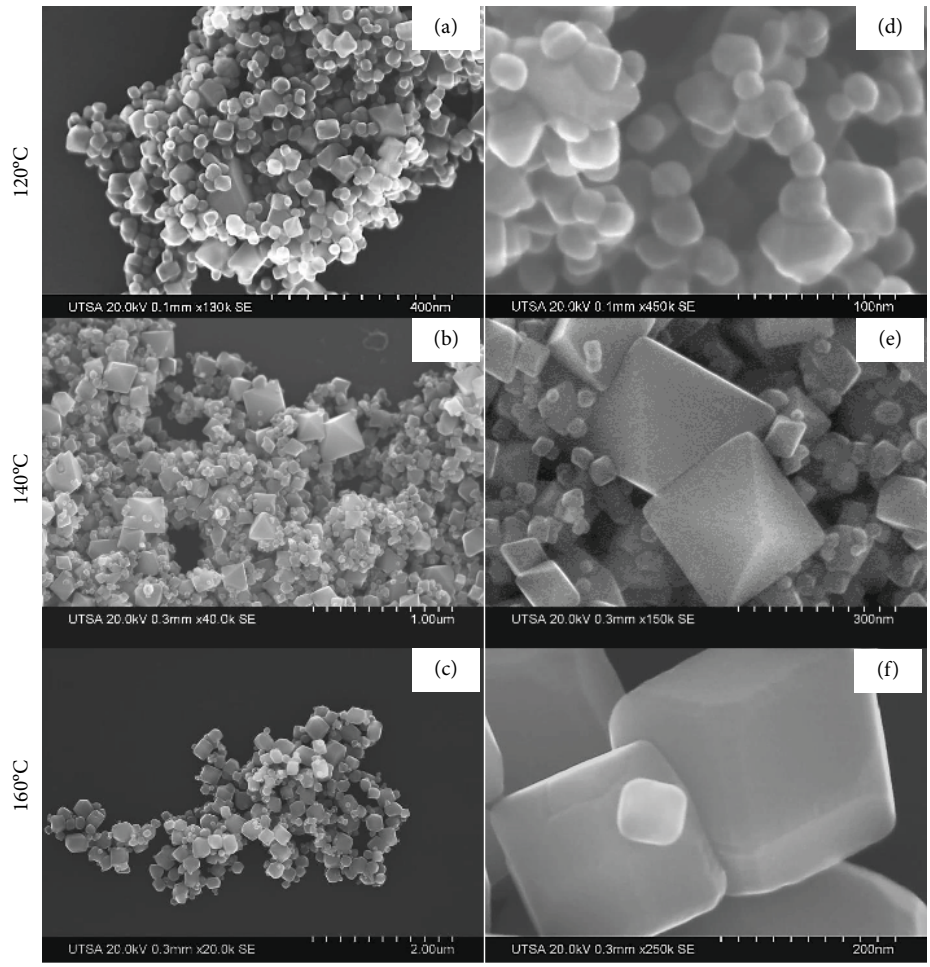

Figure 4: SEM images of magnetite nanoparticles at different temperatures. (a, d) 120°C. (b, e) 140°C. (c, f) 160°C.

microscopic techniques are complementary. This is due to SEM working at a lower resolution so it can be used to observe the samples in a larger scale, which can lead to a statistical perspective; whereas through TEM, which works at much lower resolutions (HRTEM), we can obtain information about crystalline growth, orientation, and morphology of single particles.

In order to explore the particle size distribution, more than 100 particles were measured in different micrographs for each sample (Figure 5). In spite of the particle shape being easy to control by changing the temperature used in this method, the size distribution was wide for all samples, from 10 to 65 nm (quasi-spheres), 15 to 465 nm (octahedrons), and 25 to 300 nm (cubes) for the magnetite obtained at 120°C, 140°C, and 160°C, respectively. These results show that the widest size range belongs to the magnetite obtained at 140°C, which is in accordance with the expected behavior of the XRD pattern of octahedron particles, as described above.

The experiments demonstrate that the temperature increase promotes a change in the morphology of the particles, as evidenced by SEM and TEM micrographs. The quasi-spheres, octahedrons, and cubes seen in the SEM micrographs on Figure 4 can also be observed in the TEM micrographs on Figure 6. Here, we can observe that all of the three synthesized Fe_3O_4 nanoparticles displayed uniform morphologies, a trait which closely relates to the temperatures used throughout the synthesis of the samples.

TEM and SEM micrographs confirm that a homogeneous shape control of the magnetite nanoparticles can be obtained with the developed synthesis method (Figures 6(a)–6(c)). The HRTEM image shown in Figure 6(d) exhibits planes with interplanar distances of 0.48 nm and 0.29 nm which correspond with the (111) and (220) reflection planes of magnetite; the interplanar distances of 0.48 nm in Figures 6(e) and 6(f) correspond to the distance associated with the (111) reflection planes of the inverse spinel structured Fe_3O_4.

Selected area electron diffraction (SAED) analysis further proves that the nanoparticles are highly crystalline magnetite nanoparticles. The electron diffraction pattern (Figure 6(g)) presents rings confirming the quasi-spherical morphology of the particles obtained at 120°C. The [111] growth axis is observed in the magnetite particles synthesized at 140°C (Figures 6(e) and 6(h)), which have an octahedral shape and, according to the literature, the (111) plane is the preferential growth axis for this type of morphology. The

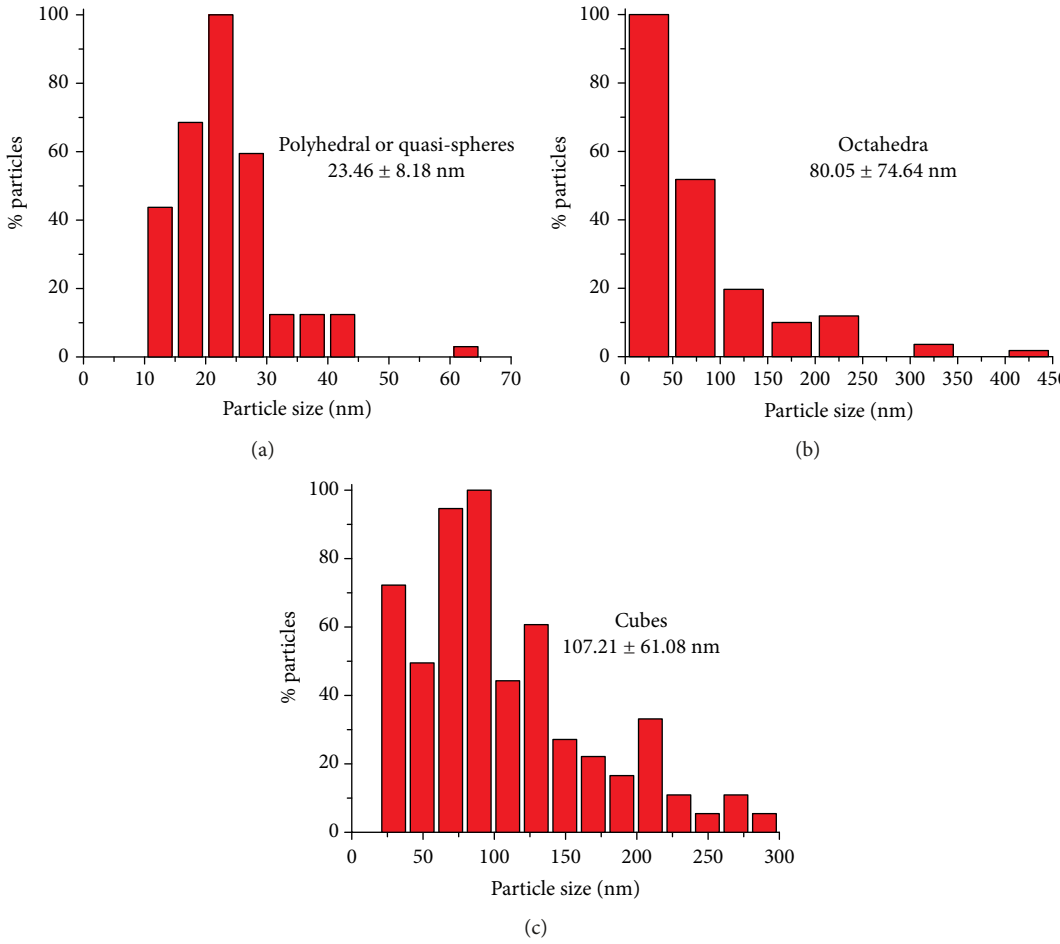

Figure 5: Size distribution of the magnetite nanoparticles at different temperatures. (a) 120°C. (b) 140°C. (c) 160°C.

corresponding SAED pattern for the Fe_3O_4 cubes of the sample synthesized at 160°C is shown in Figure 6(i), which indicates the orientation of the cubes to be in the (111) plane.

The formation of nanoparticles with controlled morphology has always been a challenge for researchers, since many variables must be controlled. Therefore, the main objective of this research is to develop an easy to replicate method of morphological control. For this reason, when controlling the variables such as concentration, precursor salts, surfactants, and solvents, the shape tuning of the nanoparticles was modified only by the reaction temperature, which is directly related to the kinetics of the reaction and the nucleation rate of the nanoparticles.

When we have a face-centered cubic crystal structure (FCC), such as with the magnetite, we can consider that the surface energy is anisotropic in the following order: $\{111\} < \{100\} < \{110\}$. Because of this, it is expected that the growth of nanostructured magnetite crystals may have a tendency to grow in an octahedral structure, considering the more stable {111} facet, as is shown in Figures 6(e) and 6(h). In Figure 6(d), which shows polyhedral and quasi-spherical morphologies, we observe the {111} and {100} facets which can be associated with the growth seeds of the octahedral nanoparticles; the {100} facets remain passivated while the temperature increases from 120°C to 140°C.

The general idea of the growing process and morphology transformation starts with chemical reaction of the iron precursors and hydrazine in the presence of PEG to form irregular and nonuniform Fe_3O_4 nanoparticles. These undergo several successive structural transformations in order to adapt to the most thermodynamically stable morphology; the transformation rate depends on the temperature, the nature of the capping agent, and the size of the particles [52, 54]. In this case, the temperature is the key in order to guide the shape.

Electron microscopy was employed to record and evaluate the evolution of quasi-spheres into octahedrons and finally into cubes. Sau and Rogach [55] reported that no spherical metal seed can be turned into octahedrons or cubes due to the similar rate of growth of the {111} and the {100} facets; this is because when all facets grow at the same rate only the particle size increases. However, if one of the facets has either a lower surface energy or is blocked by capping agents, its growth rate will be less than that of the other facet allowing the change in morphology. However, the magnetic nanoparticles show {111} as their external facet, as it is the most compact and the most stable facet. Furthermore, it is possible that octahedron morphologies could be destabilized enough at {111}, when the temperature increases from 140°C to 160°C, to allow the coalescence between particles and to

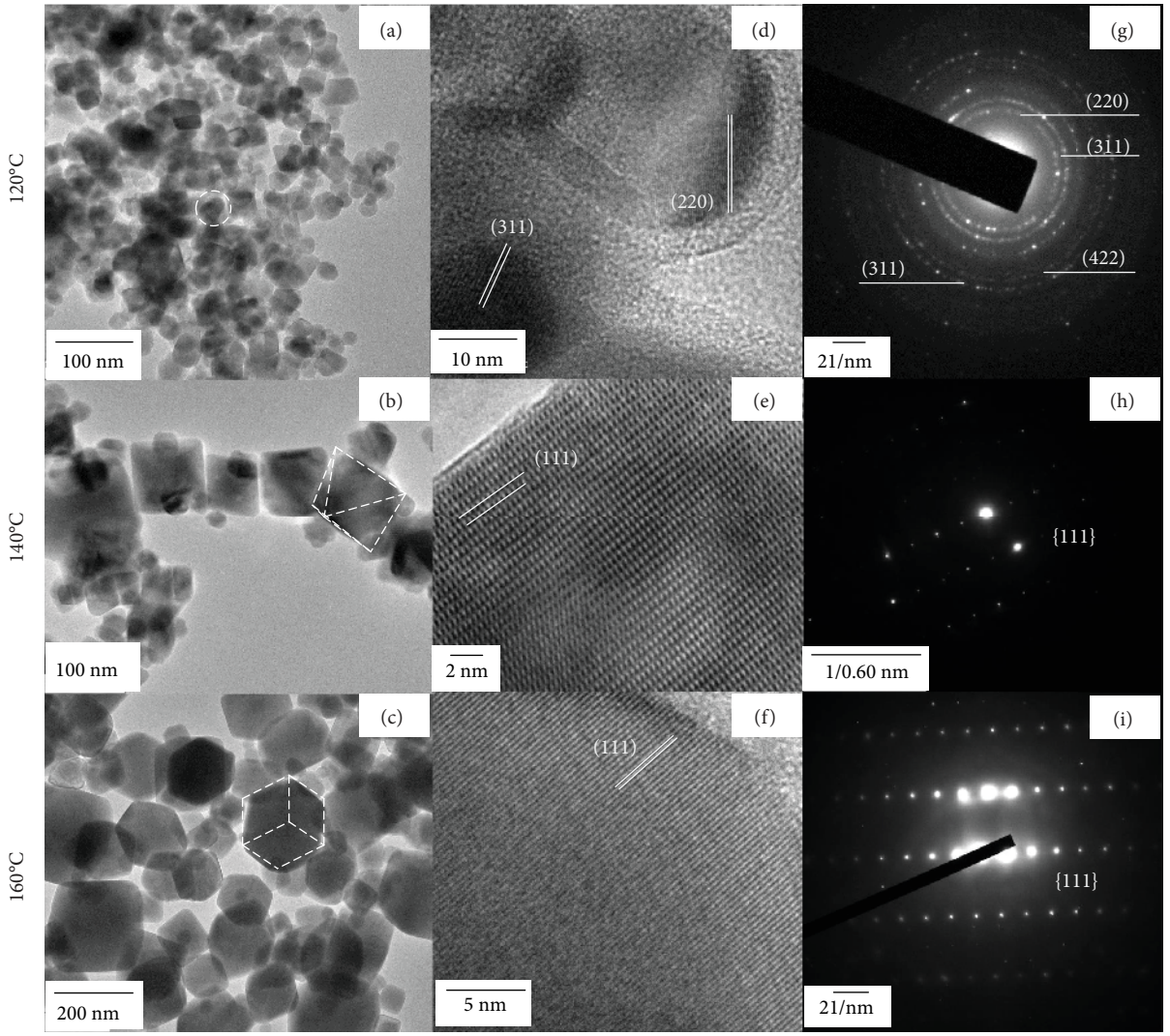

Figure 6: Micrographs of the magnetite nanoparticles at different temperatures. (a, b, c) TEM. (d, e, f) HRTEM. (g, h, i) SAED.

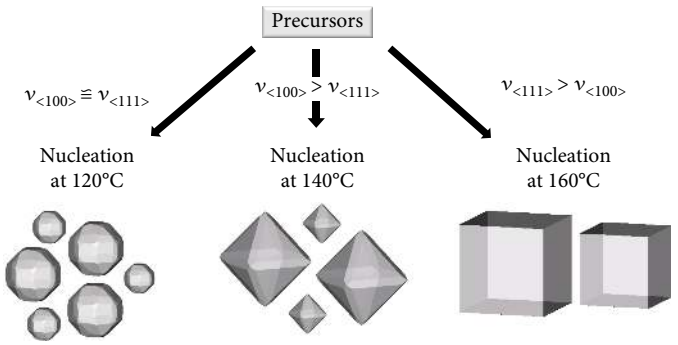

Figure 7: Schematic of the possible growth of nanoparticles of synthesized nanoparticles.

produce higher nanostructures with a cubic shape. Yet, the {111} facet remains as the external one. All the same, lengthy studies about the mechanism of shape transformation, during and after hydrothermal synthesis, have been considered within the reach of this investigation. In Figure 7, a schematic of the possible processes of the changes in the morphology of the magnetite nanoparticles, obtained with our synthesis, is presented.

3.5. Magnetic Measurement. The M-H loops of Fe_3O_4 nanoparticles synthesized at different temperatures were measured at room temperature (Figure 8). The specific

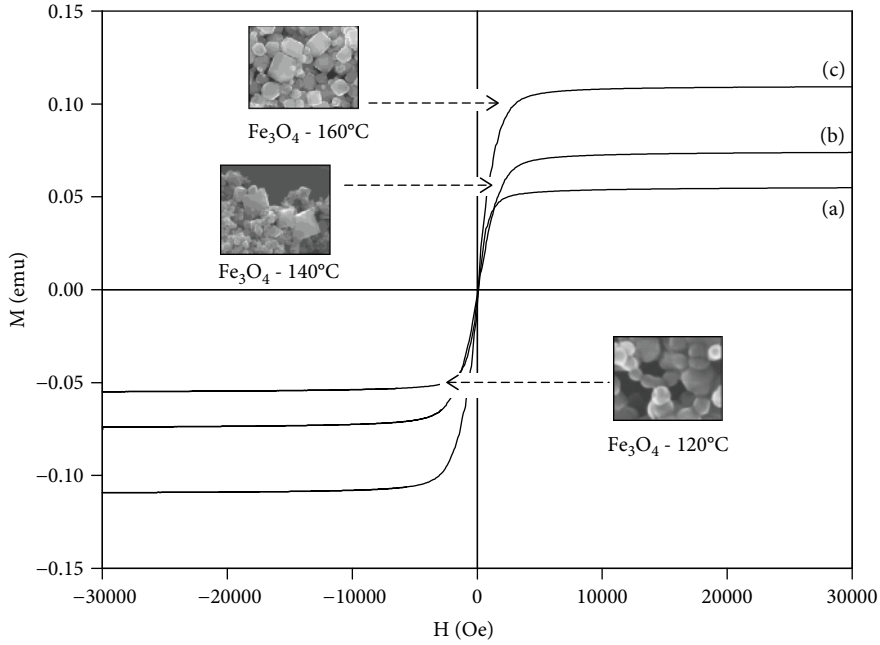

Figure 8: Magnetization curves at room temperature of Fe_3O_4 nanoparticles. (a) 120°C. (b) 140°C. (c) 160°C.

saturation magnetization (Ms) of the quasi-spherical nanoparticles obtained at 120°C is 52.71 emu/g; of the octahedrons obtained at 140°C, Ms is 73.23 emu/g; lastly, for the cubes obtained at 160°C, Ms is 107.57 emu/g. The Ms is related to size; if the nanoparticle size is increased, the Ms will increase as well. This phenomenon was observed in the magnetization curves (Figure 8) where the Ms of the cubes is higher than that of the polyhedral nanoparticles.

Another reason for the increased saturation of the magnetization in the case of Fe_3O_4 cubes may be related to the increased crystallinity (Figures 6(c), 6(f), and 6(i)), especially when comparing these results with the quasi-spherical nanoparticles, which have a lower crystallinity (Figures 6(a), 6(d), and 6(g)). Consequently, both the shape and larger size of the crystals in the cubic magnetite nanoparticles caused a significantly higher magnetization value. For these reasons, the increase in the magnetic properties may be attributed to both the increase in the size and the crystallinity of the Fe_3O_4 nanoparticles, as well as the morphology obtained by increasing the temperature synthesis from 120°C to 160°C.

In addition, it was reported that Fe_3O_4 nanoparticles smaller than 20 nm exhibit superparamagnetism because they contain a single domain with a single magnetic moment with an average Ms value of 50–60 emu/g; thus, the particles obtained from the synthesis at 120°C, in which a value of 52.71 emu/g is observed, have a superparamagnetic behavior. The coercivity (Hc) for the polyhedral, octahedron, and cubic nanoparticles is 36 Oe, 48 Oe, and 59 Oe, respectively. In general, the coercivity of magnetic materials depends on the size, morphology, and crystalline anisotropy, and were the size of the particles to increase, the coercivity would increase as well due to the particle exceeding its superparamagnetic limits (~20 nm).

3.6. Antibacterial Activity. The results of the antibacterial broth microdilution test can be seen in Figure 9. All of the concentrations tested of the different Fe_3O_4 nanoparticles (quasi-spheres, octahedrons, and cubes) showed turbidity, which translates into a low antibacterial effect. Only the Fe_3O_4 cubes showed a greater reduction of bacterial growth. *S. aureus*, *E. coli*, and *E. faecalis* showed a reduction of 54.19%, 36.12%, and 20.92%, respectively, at the highest tested concentration (5 mg/mL). However, in no case was the minimum inhibitory concentration achieved (reduction of the inoculum to less than 95%).

A potential field, which has been postulated for the application of iron oxide NPs, is a bactericidal drug. There are few reports in which the antibacterial effect is argued; particle internalization through the bacterial cell membrane is a common antibacterial mechanism. Arokiyaraj et al. [56] prepared iron oxide NPs treated with ethanoic extract of *A. mexicana* which showed a higher activity against *E. coli* and *P. mirabilis* than iron oxide NPs alone, but they attribute it to the size of the nanoparticles (less than 20 nm). In fact, this pathway is strongly dependent on particle size [57], so this mechanism is unlikely to explain the antibacterial effects of Fe_3O_4 nanoparticles with octahedral and cubic morphology.

After testing, results show a slight increase in antibacterial effect of the spheres when compared to the octahedral nanoparticles, which could be attributed to the average size of the particles. While the spheres are considerably smaller than the octahedrons, it is possible that at least a fraction of the total spheres (those with smaller size than 20 nm) are internalized in the bacteria, causing alterations in the cellular metabolism and leading to death. On the other hand, the antibacterial activity of octahedrons and cubes could be explained as a result of the edges and vertexes present in the nanoparticles. The shape-dependent activity has been

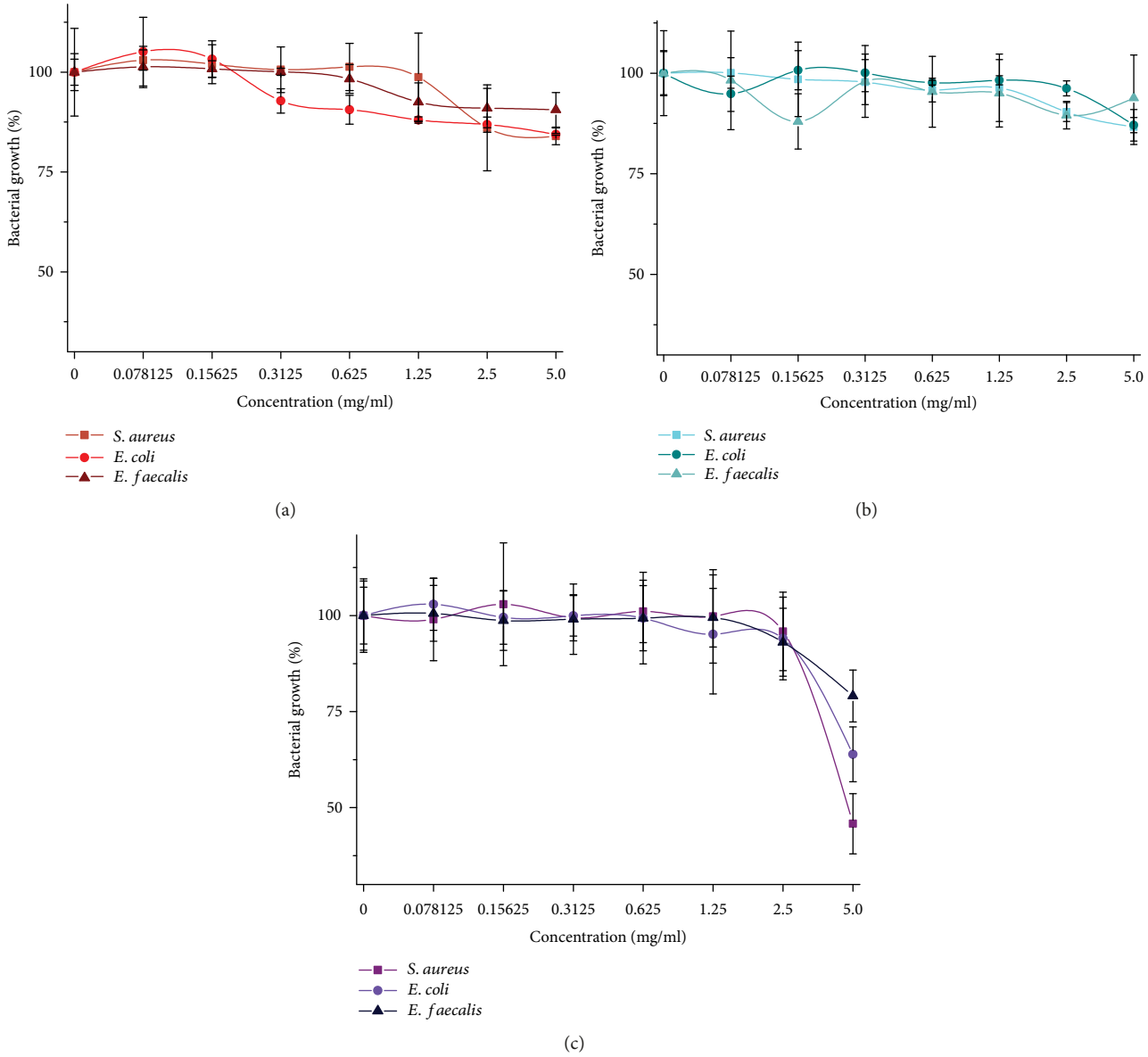

Figure 9: Graph of dilution broth test against *S. aureus*, *E. coli*, and *E. faecalis* using Fe_3O_4 nanoparticles. (a) 120°C. (b) 140°C. (c) 160°C.

explained in terms of the percent of active facets in the nanostructures. This geometric shape may contribute in the way of harming bacterial cell walls, causing cellular membrane disruption [58].

It has been reported that iron oxide NPs exhibit bacterial growth inhibition properties on a wide spectrum of bacterial species mainly by generating reactive oxygen species (ROS) from water or the environment [59]. However, in the present study, the antibacterial activity of Fe_3O_4 nanoparticles shows a low level of efficiency. It is likely that the ligand used (PEG) for nanoparticle stabilizing has had a negative effect on ROS generation, which is prevented if the Fe_3O_4 is not in contact with the medium. According to the reports by El-Sigeny and Abou Taleb, [60] the ability of the nanoparticles of Fe_3O_4 to produce ROS could depend on the stabilizing agent used; in their results, the antibacterial effect changed markedly according to this variable.

Magnetic biomaterials provide the ability to be directed and concentrated within the target tissue by means of an external magnetic field and to be removed once therapy was completed [61]. Due to this, furthermore studies are necessary in the future to allow a better iron oxide nanoparticle application in the biomedical field.

3.7. Cytotoxicity Evaluation. According to the MTT test, following the ISO 10990-5 classification for cytotoxicity, all the morphologies of the magnetite NPs were found "noncytotoxic" and only those that were below 75% of relative cell viability (at the highest dose tested) are classified as slightly cytotoxic (see Figure 10). So, it can be said that in general all the nanoparticles tested in the present study were biocompatible.

It has been shown that iron oxide nanoparticles are biocompatible and biodegradable. Due to this, such NPs have

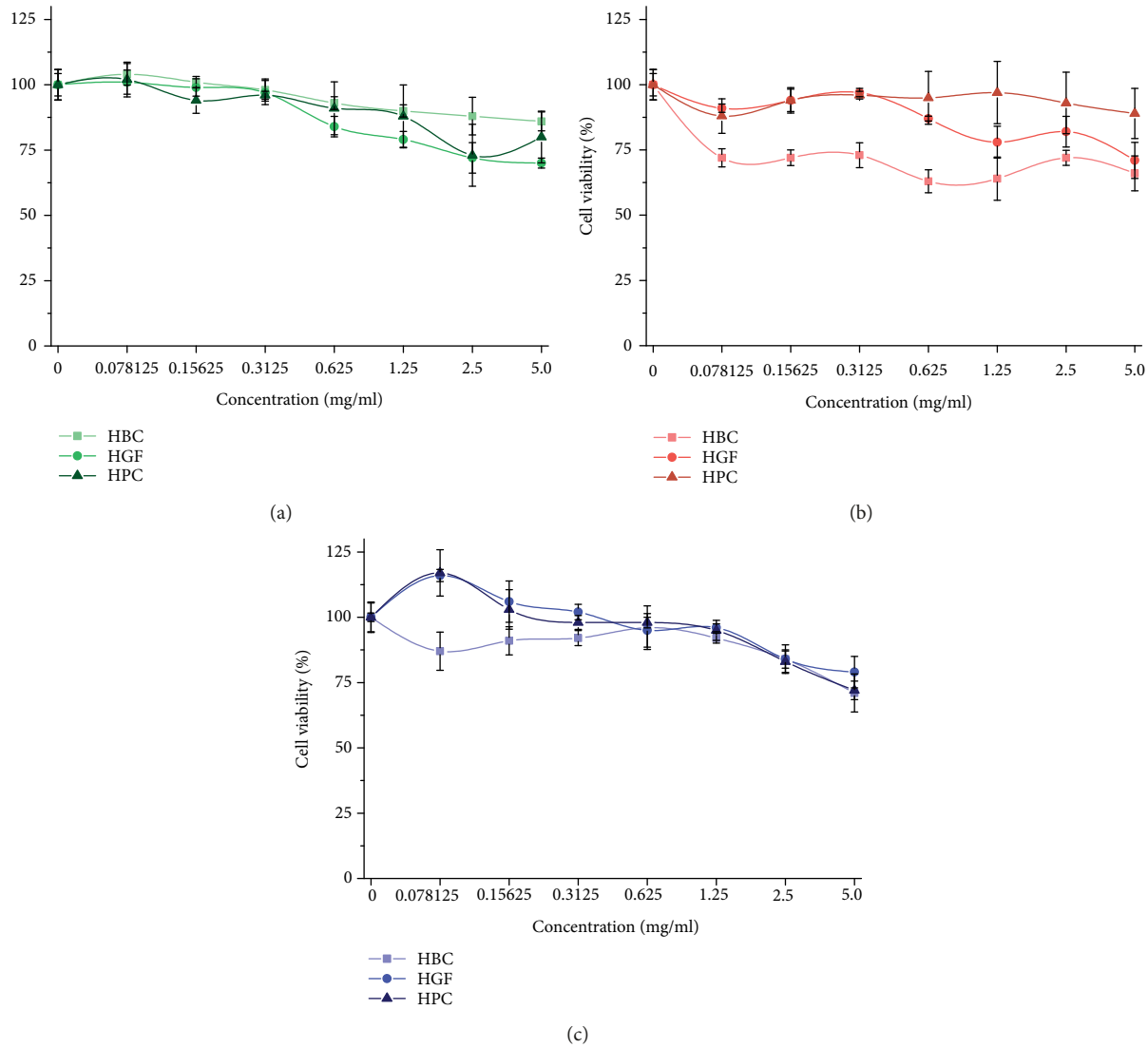

Figure 10: Graph of cell viability for human gingival fibroblast (HGF), human pulp cells (HPC), and human bone cells (HBC) in direct contact with magnetite NPs. (a) 120°C. (b) 140°C. (c) 160°C.

been studied for biomedical purposes. In a study performed by Yaaghoobi et al. [62], the toxicity of commercial and biosynthesized iron oxide NPs on peripheral blood cells was evaluated. In their study, the iron oxide NPs obtained by biosynthesis did not induce any morphological changes on peripheral blood cells. Some adverse effects of iron oxide NPs depend on their phase composition, such as Fe_3O_4, γ-Fe_2O_3, or Fe_2O_3. While γ-Fe_2O_3 nanoparticles exhibit no apparent cytotoxicity, the Fe_3O_4 nanoparticles containing Fe^{2+} ions were found to be cytotoxic [63]. Studying how the nanoparticles are recognized from a biological approach is vital to improve their design and potential applications. However, it has been suggested that iron oxide NPs (and nanoparticles in general) enter into cells via endocytosis, a mechanism that leads to cellular death due to the massive internalization [64]. One of the major routes affecting the survival of nanoparticles in circulation is their recognition by the reticuloendothelial system [65]. This recognition by the innate immune system would induce to phagocytosis of the foreign antigen and the activation of specific antigens mediated by B-2 cells, initiating the adaptive response [66]. The acquired antibodies allow the process of particle clearance more efficient by opsonization, activation of complementary system, and by the induction of the inflammatory response [67, 68].

Another important topic is the nanoparticle size. It seems increasingly evident that the size is critical for their biocompatibility and their subsequent degradation. There is evidence that accumulation in the spleen and liver depends directly on the particle size. When nanoparticles are intravenously or intraperitoneally injected, inorganic and organic nanoparticles are mainly sequestered in the liver and spleen. Iron oxide NPs with a 150 nm diameter are accumulated in the liver and the spleen, whereas particles having sizes below 10–15 nm are selectively filtered by the renal system and eliminated from the organism [69, 70]. Another main concern is that the release of free iron from the magnetite core could be cytotoxic due to its catalytic

function in the production of reactive oxygen species in the course of the Fenton reaction [71].

There are, in fact, magnetic iron oxide nanoparticles already in the market. They are used as contrast agents during magnetic resonance imaging (MRI) scans such as Feridexs, (Advanced Magnetics, USA, Endorem®, Guerbet, France; dextran-coated, hydrodynamic diameter of 120–180 nm), Ferumoxtran-10 (Combidex® in USA, Sinerem® in Europe), among others [72]. Endorem®, as well as carboxydextran-coated Ferucarbotran®, was specifically approved for liver MRIs, due to affinity of the iron oxide nanoparticles for their rapid opsonization followed by sequestration by Kupffer cells in the liver upon intravenous injection; as a result, their application is limited to diseases related to phagocytic cells [73]. In contrast, it was found that even high concentrations of Ferumoxtran-10 are not acutely toxic to human macrophages *in vitro*; they do not produce proinflammatory cytokines or superoxide anions; they are not chemotactic nor do they interfere with Fc-receptor-mediated phagocytosis [74]. Still, more experimental research and *in vivo* studies are required to advance composition optimization and to improve the efficiency of these NPs for imaging and drug delivery applications. More thorough investigation is required to further understand the precise mechanisms involved in the detachment of these molecules from the nanoparticles (the zeta potential charge of the bare nanoparticles which impacts their adsorption of lipoproteins in systemic circulation, nonspecific binding, their subsequent clearance and *in vivo* transport [75, 76]), their biodistribution, and their elimination mechanisms.

Some studies indicate that the clearance of iron oxide NPs requires between 3 and 7 weeks when released in an organism, which implies that the NPs must be tracked for long periods of time [77, 78]. The clearance time is not completely agreed upon, possibly due to the differences in the sizes of the iron oxide particles and the type of coating or functionalizing molecules used. The current data point out that to prevent this mechanism the coating/functionalization of the nanoparticles is required. For example, dextran is routinely used for coating iron oxide NPs, because of its high affinity to them. This coating provides steric stability to the particles, which prevents their aggregation in an aqueous continuous phase [67]. A certain concern about the potential immunogenic response of coating iron oxide NPs was found [79]; however, these NPs are more cytotoxic without coating.

In the present study, PEG was used as a particle stabilizer, which allows the nanoparticles to be dissolved completely in an aqueous medium along with the cell culture. The iron oxide nanoparticles coated with PEG showed adequate biocompatibility. Although the MTT assay is a reliable test *in vitro*, these results must be confirmed in an *in vivo* animal model. This would allow a possible comparison with the aforementioned *in vivo* studies.

4. Conclusion

In summary, we have shown that by modifying only the temperature of the syntheses while using the hydrothermal method, a good morphological control of nanostructured magnetite can be successfully obtained, where morphology is an essential requirement to adjust magnetic properties in different potential applications. As a result, it has been possible to obtain quasi-spheres, octahedrons, and cubes in the nanometric regime, by adjusting the temperature to 120°C, 140°C, and 160°C, respectively, without the modification of any other synthesis parameters, thus obtaining a simple, economical, and scalable method for obtaining magnetic nanoparticles. The antibacterial activity of magnetite NPs tested shows a low level of efficiency. However, the cytotoxicity was "slightly cytotoxic" and "noncytotoxic." So the magnetite nanoparticles could potentially be used in the biomedical field.

Data Availability

The data used to support the findings of this study are available from the corresponding author upon request.

Conflicts of Interest

The authors declare that they have no conflicts of interest.

Acknowledgments

The authors acknowledge the Kleberg Advanced Microscopy Center (KAMiC) and NIH RCMI Nanotechnology and Human Health Core (Grant 5G12RR013646-12) at University of Texas at San Antonio for the support with electron microscopy. The authors gratefully acknowledge Dr. Elizande-Galindo and Dr. Farias Mancilla from UACJ for their technical support with magnetic measurements. This research was funded by UAEM Grant 3688/20147CIB and CONACYT Grant 280518. The authors thank the Cátedras-CONACYT program and the Facultad de Odontología, Universidad Autónoma Benito Juárez de Oaxaca, for their support. The authors also thank the financial support from DGAPA-UNAM: PAPIIT-IA205518 and PAPIME-PE208518.

References

[1] X. Yao, K. Sabyrov, T. Klein, R. Lee Penn, and T. S. Wiedmann, "Evaluation of magnetic heating of asymmetric magnetite particles," *Journal of Magnetism and Magnetic Materials*, vol. 381, pp. 21–27, 2015.

[2] J. Wang, A. Munir, Z. Zhu, and H. S. Zhou, "Magnetic nanoparticle enhanced surface plasmon resonance sensing and its application for the ultrasensitive detection of magnetic nanoparticle-enriched small molecules," *Analytical Chemistry*, vol. 82, no. 16, pp. 6782–6789, 2010.

[3] A. L. Swindle, A. S. E. Madden, I. M. Cozzarelli, and M. Benamara, "Size-dependent reactivity of magnetite nanoparticles: a field-laboratory comparison," *Environmental Science & Technology*, vol. 48, no. 19, pp. 11413–11420, 2014.

[4] P. Majewski and B. Thierry, "Functionalized magnetite nanoparticles-synthesis, properties, and bio-applications," *Critical Reviews in Solid State and Materials Sciences*, vol. 32, no. 3-4, pp. 203–215, 2007.

[5] K. Atacan, B. Çakıroğlu, and M. Özacar, "Covalent immobilization of trypsin onto modified magnetite nanoparticles and its application for casein digestion," *International Journal of Biological Macromolecules*, vol. 97, pp. 148–155, 2017.

[6] M. Aghazadeh, I. Karimzadeh, and M. R. Ganjali, "Electrochemical evaluation of the performance of cathodically grown ultra-fine magnetite nanoparticles as electrode material for supercapacitor applications," *Journal of Materials Science: Materials in Electronics*, vol. 28, no. 18, pp. 13532–13539, 2017.

[7] A. Ruiz, G. Salas, M. Calero et al., "Short-chain PEG molecules strongly bound to magnetic nanoparticle for MRI long circulating agents," *Acta Biomaterialia*, vol. 9, no. 5, pp. 6421–6430, 2013.

[8] M. Mahmoudi, A. Simchi, M. Imani et al., "A new approach for the in vitro identification of the cytotoxicity of superparamagnetic iron oxide nanoparticles," *Colloids and Surfaces B: Biointerfaces*, vol. 75, no. 1, pp. 300–309, 2010.

[9] M. Fazilati, "Folate decorated magnetite nanoparticles: synthesis and targeted therapy against ovarian cancer," *Cell Biology International*, vol. 38, no. 2, pp. 154–163, 2013.

[10] M. Ravichandran, S. Velumani, and J. T. Ramirez, "Water-dispersible magnetite nanoparticles as T_2 MR imaging contrast agent," *Biomedical Physics & Engineering Express*, vol. 3, no. 1, article 015011, 2017.

[11] K. Petcharoen and A. Sirivat, "Synthesis and characterization of magnetite nanoparticles via the chemical co-precipitation method," *Materials Science and Engineering: B*, vol. 177, no. 5, pp. 421–427, 2012.

[12] R. Valenzuela, M. C. Fuentes, C. Parra et al., "Influence of stirring velocity on the synthesis of magnetite nanoparticles (Fe_3O_4) by the co-precipitation method," *Journal of Alloys and Compounds*, vol. 488, no. 1, pp. 227–231, 2009.

[13] X. Wei and R. C. Viadero Jr, "Synthesis of magnetite nanoparticles with ferric iron recovered from acid mine drainage: implications for environmental engineering," *Colloids and Surfaces A: Physicochemical and Engineering Aspects*, vol. 294, no. 1-3, pp. 280–286, 2007.

[14] D. Maity, S. N. Kale, R. Kaul-Ghanekar, J. M. Xue, and J. Ding, "Studies of magnetite nanoparticles synthesized by thermal decomposition of iron (III) acetylacetonate in tri(ethylene glycol)," *Journal of Magnetism and Magnetic Materials*, vol. 321, no. 19, pp. 3093–3098, 2009.

[15] D. Maity, S. G. Choo, J. Yi, J. Ding, and J. M. Xue, "Synthesis of magnetite nanoparticles via a solvent-free thermal decomposition route," *Journal of Magnetism and Magnetic Materials*, vol. 321, no. 9, pp. 1256–1259, 2009.

[16] L. Zhang, R. He, and H. C. Gu, "Oleic acid coating on the monodisperse magnetite nanoparticles," *Applied Surface Science*, vol. 253, no. 5, pp. 2611–2617, 2006.

[17] R. N. Panda, N. S. Gajbhiye, and G. Balaji, "Magnetic properties of interacting single domain Fe_3O_4 particles," *Journal of Alloys and Compounds*, vol. 326, no. 1-2, pp. 50–53, 2001.

[18] H. P. Shao, Y. M. Tan, T. Lin, and Z. M. Guo, "Size-controlled synthesis of magnetite nanoparticles from iron acetate by thermal decomposition," *Applied Mechanics and Materials*, vol. 217-219, pp. 256–259, 2012.

[19] P. Ou, G. Xu, C. Xu, Y. Zhang, X. Hou, and G. Han, "Synthesis and characterization of magnetite nanoparticles by a simple solvothermal method," *Materials Science-Poland*, vol. 28, no. 4, 2010.

[20] Y. Zhan, R. Zhao, F. Meng et al., "Oriented growth of magnetite along the carbon nanotubes via covalently bonded method in a simple solvothermal system," *Materials Science and Engineering: B*, vol. 176, no. 10, pp. 779–784, 2011.

[21] A. Rabenau, "The role of hydrothermal synthesis in preparative chemistry," *Angewandte Chemie International Edition*, vol. 24, no. 12, pp. 1026–1040, 1985.

[22] P. Coppola, F. G. da Silva, G. Gomide et al., "Hydrothermal synthesis of mixed zinc–cobalt ferrite nanoparticles: structural and magnetic properties," *Journal of Nanoparticle Research*, vol. 18, no. 5, p. 138, 2016.

[23] K. Byrappa and M. Yoshimura, *Handbook of Hydrothermal Technology*, Elsevier, 2012.

[24] J.-H. Wu, S. P. Ko, H.-L. Liu, S. Kim, J.-S. Ju, and Y. K. Kim, "Sub 5 nm magnetite nanoparticles: synthesis, microstructure, and magnetic properties," *Materials Letters*, vol. 61, no. 14-15, pp. 3124–3129, 2007.

[25] L. Shen, Y. Qiao, Y. Guo et al., "Facile co-precipitation synthesis of shape-controlled magnetite nanoparticles," *Ceramics International*, vol. 40, no. 1, pp. 1519–1524, 2014.

[26] M. Wang, M. L. Peng, W. Cheng, Y. L. Cui, and C. Chen, "A novel approach for transferring oleic acid capped iron oxide nanoparticles to water phase," *Journal of Nanoscience and Nanotechnology*, vol. 11, no. 4, pp. 3688–3691, 2011.

[27] J. Zhang, S. Rana, R. S. Srivastava, and R. D. K. Misra, "On the chemical synthesis and drug delivery response of folate receptor-activated, polyethylene glycol-functionalized magnetite nanoparticles," *Acta Biomaterialia*, vol. 4, no. 1, pp. 40–48, 2008.

[28] P. Majewski and B. Thierry, "Functionalized magnetite nanoparticles—synthesis, properties, and bio-applications," *Critical Reviews in Solid State and Materials Sciences*, vol. 32, no. 3-4, pp. 203–215, 2007.

[29] B. Feng, R. Y. Hong, L. S. Wang et al., "Synthesis of Fe_3O_4/APTES/PEG diacid functionalized magnetic nanoparticles for MR imaging," *Colloids and Surfaces A: Physicochemical and Engineering Aspects*, vol. 328, no. 1-3, pp. 52–59, 2008.

[30] L. Hou, Q. Zhang, F. Jérôme, D. Duprez, H. Zhang, and S. Royer, "Shape-controlled nanostructured magnetite-type materials as highly efficient Fenton catalysts," *Applied Catalysis B: Environmental*, vol. 144, pp. 739–749, 2014.

[31] Y. Li, R. Jiang, T. Liu, H. Lv, and X. Zhang, "Single-microemulsion-based solvothermal synthesis of magnetite microflowers," *Ceramics International*, vol. 40, no. 3, pp. 4791–4795, 2014.

[32] J. Sato, M. Kobayashi, H. Kato, T. Miyazaki, and M. Kakihana, "Hydrothermal synthesis of magnetite particles with uncommon crystal facets," *Journal of Asian Ceramic Societies*, vol. 2, no. 3, pp. 258–262, 2014.

[33] D. Ramimoghadam, S. Bagheri, and S. B. A. Hamid, "In-situ precipitation of ultra-stable nano-magnetite slurry," *Journal of Magnetism and Magnetic Materials*, vol. 379, pp. 74–79, 2015.

[34] T. J. Daou, G. Pourroy, S. Bégin-Colin et al., "Hydrothermal synthesis of monodisperse magnetite nanoparticles," *Chemistry of Materials*, vol. 18, no. 18, pp. 4399–4404, 2006.

[35] Z. Xu, C. Shen, Y. Hou, H. Gao, and S. Sun, "Oleylamine as both reducing agent and stabilizer in a facile synthesis of magnetite nanoparticles," *Chemistry of Materials*, vol. 21, no. 9, pp. 1778–1780, 2009.

[36] X. Sun, C. Zheng, F. Zhang et al., "Size-controlled synthesis of magnetite (Fe_3O_4) nanoparticles coated with glucose and

gluconic acid from a single Fe(III) precursor by a sucrose bifunctional hydrothermal method," *The Journal of Physical Chemistry C*, vol. 113, no. 36, pp. 16002–16008, 2009.

[37] H. Zhang and G. Zhu, "One-step hydrothermal synthesis of magnetic Fe_3O_4 nanoparticles immobilized on polyamide fabric," *Applied Surface Science*, vol. 258, no. 11, pp. 4952–4959, 2012.

[38] M. Arruebo, R. Fernández-Pacheco, M. R. Ibarra, and J. Santamaría, "Magnetic nanoparticles for drug delivery," *Nano Today*, vol. 2, no. 3, pp. 22–32, 2007.

[39] N. Lee and T. Hyeon, "Designed synthesis of uniformly sized iron oxide nanoparticles for efficient magnetic resonance imaging contrast agents," *Chemical Society Reviews*, vol. 41, no. 7, pp. 2575–2589, 2012.

[40] M. Bañobre-López, A. Teijeiro, and J. Rivas, "Magnetic nanoparticle-based hyperthermia for cancer treatment," *Reports of Practical Oncology & Radiotherapy*, vol. 18, no. 6, pp. 397–400, 2013.

[41] H. Wiogo, M. Lim, P. Munroe, and R. Amal, "Understanding the formation of iron oxide nanoparticles with acicular structure from iron(III) chloride and hydrazine monohydrate," *Crystal Growth & Design*, vol. 11, no. 5, pp. 1689–1696, 2011.

[42] L. Argueta-Figueroa, N. Torres-Gómez, R. García-Contreras et al., "Hydrothermal synthesis of pyrrhotite (Fe_x-1S) nanoplates and their antibacterial, cytotoxic activity study," *Progress in Natural Science: Materials International*, vol. 28, no. 4, pp. 447–455, 2018.

[43] M. A. Wikler, *Methods for Dilution Antimicrobial Susceptibility Tests for Bacteria That Grow Aerobically*, National Committee for Clinical Laboratory Standards, 2009.

[44] O. N. Shebanova and P. Lazor, "Raman study of magnetite (Fe_3O_4): laser-induced thermal effects and oxidation," *Journal of Raman Spectroscopy*, vol. 34, no. 11, pp. 845–852, 2003.

[45] O. N. Shebanova and P. Lazor, "Raman spectroscopic study of magnetite ($FeFe_2O_4$): a new assignment for the vibrational spectrum," *Journal of Solid State Chemistry*, vol. 174, no. 2, pp. 424–430, 2003.

[46] N. Boucherit, A. Hugot-Le Goff, and S. Joiret, "Raman studies of corrosion films grown on Fe and Fe-6Mo in pitting conditions," *Corrosion Science*, vol. 32, no. 5-6, pp. 497–507, 1991.

[47] T. Ohtsuka, K. Kubo, and N. Sato, "Raman spectroscopy of thin corrosion films on iron at 100 to 150 C in air," *Corrosion*, vol. 42, no. 8, pp. 476–481, 1986.

[48] D. Thierry, D. Persson, C. Leygraf, N. Boucherit, and A. Hugot-Le Goff, "Raman spectroscopy and XPS investigations of anodic corrosion films formed on FeMo alloys in alkaline solutions," *Corrosion Science*, vol. 32, no. 3, pp. 273–284, 1991.

[49] D. L. A. De Faria, S. Venâncio Silva, and M. T. De Oliveira, "Raman microspectroscopy of some iron oxides and oxyhydroxides," *Journal of Raman Spectroscopy*, vol. 28, no. 11, pp. 873–878, 1997.

[50] J. M. Li, A. C. H. Huan, L. Wang, Y. W. Du, and D. Feng, "Interface effects on magnetoresistance and magnetic-field-reduced Raman scattering in magnetite," *Physical Review B*, vol. 61, no. 10, pp. 6876–6878, 2000.

[51] D. Bersani, P. P. Lottici, and A. Montenero, "Micro-Raman investigation of iron oxide films and powders produced by sol–gel syntheses," *Journal of Raman Spectroscopy*, vol. 30, no. 5, pp. 355–360, 1999.

[52] R. M. Cornell and U. Schwertmann, *The Iron Oxides: Structure, Properties, Reactions, Occurrences and Uses*, John Wiley & Sons, Second edition, 2003.

[53] H. Borchert, E. V. Shevchenko, A. Robert et al., "Determination of nanocrystal sizes: a comparison of TEM, SAXS, and XRD studies of highly monodisperse CoPt3 particles," *Langmuir*, vol. 21, no. 5, pp. 1931–1936, 2005.

[54] M. J. Yacamán, J. A. Ascencio, H. B. Liu, and J. Gardea-Torresdey, "Structure shape and stability of nanometric sized particles," *Journal of Vacuum Science & Technology B: Microelectronics and Nanometer Structures Processing, Measurement, and Phenomena*, vol. 19, no. 4, pp. 1091–1103, 2001.

[55] T. K. Sau and A. L. Rogach, "Nonspherical noble metal nanoparticles: colloid-chemical synthesis and morphology control," *Advanced Materials*, vol. 22, no. 16, pp. 1781–1804, 2010.

[56] S. Arokiyaraj, M. Saravanan, N. K. Udaya Prakash, M. Valan Arasu, B. Vijayakumar, and S. Vincent, "Enhanced antibacterial activity of iron oxide magnetic nanoparticles treated with Argemone mexicana L. leaf extract: an in vitro study," *Materials Research Bulletin*, vol. 48, no. 9, pp. 3323–3327, 2013.

[57] J. Rejman, V. Oberle, I. S. Zuhorn, and D. Hoekstra, "Size-dependent internalization of particles via the pathways of clathrin-and caveolae-mediated endocytosis," *Biochemical Journal*, vol. 377, no. 1, pp. 159–169, 2004.

[58] M. J. Hajipour, K. M. Fromm, A. Akbar Ashkarran et al., "Antibacterial properties of nanoparticles," *Trends in Biotechnology*, vol. 30, no. 10, pp. 499–511, 2012.

[59] N. Tran, A. Mir, D. Mallik, A. Sinha, S. Nayar, and T. Webster, "Bactericidal effect of iron oxide nanoparticles on *Staphylococcus aureus*," *International Journal of Nanomedicine*, vol. 2010, no. 5, pp. 277–283, 2010.

[60] S. M. El-Sigeny and M. F. Abou Taleb, "Synthesis, characterization, and application of dendrimer modified magnetite nanoparticles as antimicrobial agent," *Life Science Journal*, vol. 12, no. 6, pp. 161–170, 2015.

[61] T. K. Indira and P. K. Lakshmi, "Magnetic nanoparticles–a review," *International Journal of Pharmaceutical Sciences and Nanotechnology*, vol. 3, no. 3, pp. 1035–1042, 2010.

[62] M. Yaaghoobi, G. Emtiazi, and R. Roghanian, "A novel approach for aerobic construction of iron oxide nanoparticles by acinetobacter radioresistens and their effects on red blood cells," *Current Nanoscience*, vol. 8, no. 2, pp. 286–291, 2012.

[63] S. Klein, A. Sommer, L. V. R. Distel, W. Neuhuber, and C. Kryschi, "Superparamagnetic iron oxide nanoparticles as radiosensitizer via enhanced reactive oxygen species formation," *Biochemical and Biophysical Research Communications*, vol. 425, no. 2, pp. 393–397, 2012.

[64] L. Kou, J. Sun, Y. Zhai, and Z. He, "The endocytosis and intracellular fate of nanomedicines: implication for rational design," *Asian Journal of Pharmaceutical Sciences*, vol. 8, no. 1, pp. 1–10, 2013.

[65] S. Shanehsazzadeh, M. A. Oghabian, F. J. Daha, M. Amanlou, and B. J. Allen, "Biodistribution of ultra small superparamagnetic iron oxide nanoparticles in BALB mice," *Journal of Radioanalytical and Nuclear Chemistry*, vol. 295, no. 2, pp. 1517–1523, 2013.

[66] G. L. Szeto and E. B. Lavik, "Materials design at the interface of nanoparticles and innate immunity," *Journal of Materials Chemistry B*, vol. 4, no. 9, pp. 1610–1618, 2016.

[67] O. Ziv, R. R. Avtalion, and S. Margel, "Immunogenicity of bioactive magnetic nanoparticles: natural and acquired antibodies," *Journal of Biomedical Materials Research Part A*, vol. 85, no. 4, pp. 1011–1021, 2008.

[68] O. Ziv, T. Lublin-Tennenbaum, and S. Margel, "Synthesis and characterization of thrombin conjugated γ-Fe_2O_3 magnetic nanoparticles for hemostasis," *Advanced Engineering Materials*, vol. 11, no. 12, pp. B251–B260, 2009.

[69] J. J. Hue, H. J. Lee, S. Jon et al., "Distribution and accumulation of Cy5. 5-labeled thermally cross-linked superparamagnetic iron oxide nanoparticles in the tissues of ICR mice," *Journal of Veterinary Science*, vol. 14, no. 4, pp. 473–479, 2013.

[70] H. Arami, A. Khandhar, D. Liggitt, and K. M. Krishnan, "In vivo delivery, pharmacokinetics, biodistribution and toxicity of iron oxide nanoparticles," *Chemical Society Reviews*, vol. 44, no. 23, pp. 8576–8607, 2015.

[71] N. Singh, G. J. S. Jenkins, R. Asadi, and S. H. Doak, "Potential toxicity of superparamagnetic iron oxide nanoparticles (SPION)," *Nano Reviews*, vol. 1, no. 1, p. 5358, 2010.

[72] D. Couto, M. Freitas, F. Carvalho, and E. Fernandes, "Iron oxide nanoparticles: an insight into their biomedical applications," *Current Medicinal Chemistry*, vol. 22, no. 15, pp. 1808–1828, 2015.

[73] S. Sharifi, H. Seyednejad, S. Laurent, F. Atyabi, A. A. Saei, and M. Mahmoudi, "Superparamagnetic iron oxide nanoparticles for in vivo molecular and cellular imaging," *Contrast Media & Molecular Imaging*, vol. 10, no. 5, pp. 329–355, 2015.

[74] K. Müller, J. N. Skepper, M. Posfai et al., "Effect of ultrasmall superparamagnetic iron oxide nanoparticles (Ferumoxtran-10) on human monocyte-macrophages in vitro," *Biomaterials*, vol. 28, no. 9, pp. 1629–1642, 2007.

[75] H. S. Han, J. D. Martin, J. Lee et al., "Spatial charge configuration regulates nanoparticle transport and binding behavior in vivo," *Angewandte Chemie International Edition*, vol. 52, no. 5, pp. 1414–1419, 2013.

[76] R. Kumar, I. Roy, T. Y. Ohulchanskky et al., "*In vivo* biodistribution and clearance studies using multimodal organically modified silica nanoparticles," *ACS Nano*, vol. 4, no. 2, pp. 699–708, 2010.

[77] T. K. Jain, M. K. Reddy, M. A. Morales, D. L. Leslie-Pelecky, and V. Labhasetwar, "Biodistribution, clearance, and biocompatibility of iron oxide magnetic nanoparticles in rats," *Molecular Pharmaceutics*, vol. 5, no. 2, pp. 316–327, 2008.

[78] P. Bourrinet, H. H. Bengele, B. Bonnemain et al., "Preclinical safety and pharmacokinetic profile of ferumoxtran-10, an ultrasmall superparamagnetic iron oxide magnetic resonance contrast agent," *Investigative Radiology*, vol. 41, no. 3, pp. 313–324, 2006.

[79] C. C. Berry, S. Wells, S. Charles, and A. S. G. Curtis, "Dextran and albumin derivatised iron oxide nanoparticles: influence on fibroblasts in vitro," *Biomaterials*, vol. 24, no. 25, pp. 4551–4557, 2003.